

Tensor network simulation of non-Markovian dynamics in organic polaritons

Javier del Pino,¹ Florian A. Y. N. Schröder,² Alex W. Chin,^{3,2} Johannes Feist,^{1,*} and Francisco J. Garcia-Vidal^{1,4,†}

¹*Departamento de Física Teórica de la Materia Condensada and Condensed Matter Physics Center (IFIMAC), Universidad Autónoma de Madrid, E-28049 Madrid, Spain*

²*Cavendish Laboratory, University of Cambridge, J. J. Thomson Avenue, Cambridge, CB3 0HE, UK*

³*Institut des NanoSciences de Paris, Sorbonne Université,*

4 place Jussieu, boîte courrier 840, 75252, PARIS Cedex 05

⁴*Donostia International Physics Center (DIPC), E-20018 Donostia/San Sebastián, Spain*

We calculate the exact many-body time dynamics of polaritonic states supported by an optical cavity filled with organic molecules. Optical, vibrational and radiative processes are treated on an equal footing employing the Time-Dependent Variational Matrix Product States algorithm. We demonstrate signatures of non-Markovian vibronic dynamics and its fingerprints in the far-field photon emission spectrum at arbitrary light-matter interaction scales, ranging from the weak to the strong coupling regimes. We analyze both the single and many-molecule cases, showing the crucial role played by the collective motion of molecular nuclei and dark states in determining the polariton dynamics and the subsequent photon emission.

Organic polaritons, formed upon hybridization of optical electromagnetic (EM) modes and Frenkel excitons of organic molecules [1–5], exist as a threefold mixture of photonic, electronic and phononic excitations. As a result, modified nuclear effects in polaritons leads to tailored material [6–8] and chemical [9–13] properties. In this regard, experiments have underlined the impact of vibronic states in the polariton time evolution, with examples in thermalization and cooling of room T condensates [14–16], thresholds in organic lasers [17, 18] and lifetimes [19–21]. First studies on the impact of vibrations on organic polariton dynamics relied on the Fermi’s golden rule within a Markovian approach [22, 23], which neglects correlations and interplay between electronic and vibrational excitations. More recently, the influence of vibronic states in the spectroscopic properties of these systems [24, 25] has been analyzed using the Holstein-Tavis-Cummings (HTC) model, in which the complex spectral density of the vibronic modes in organic molecules is modelled by a single phonon mode.

In this Letter we simulate the temporal dynamics of the polaritons supported by an optical microcavity filled with an ensemble of prototypical organic molecules (Rhodamine 800), as sketched in Fig. 1a. In our approach, nuclear, electronic and photonic processes are treated fully and on equal footing by employing the Time-Dependent Variational Matrix Product States algorithm (TDVMPS), which can provide quasi-exact solutions of open quantum system dynamics by truncating the maximum entanglement between different system components [26–30]. Our fundamental study reveals a variety of regimes for the time evolution of the polariton populations, which experience vibration-assisted dynamics that translate into distinct far-field emission fingerprints. We observe clear signatures of non-Markovian behavior in the whole range of light-matter coupling, both for single and multiple molecules coupled to an EM cavity mode. We find that the full

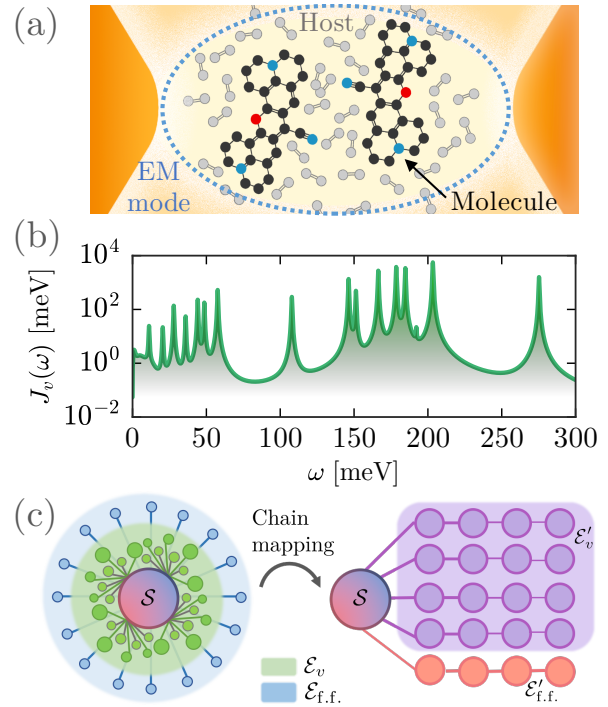


FIG. 1. (a) Sketch of a molecular ensemble interacting with a confined EM resonance (dashed region) and with the host environment (grey circles). (b) Vibrational spectral density for Rhodamine 800 molecule. (c) Scheme illustrating the mapping of the vibrational modes yielding the multi-chain Hamiltonian used in the simulations.

vibrational structure of the molecules has to be treated for a complete understanding of the interplay between excitons, phonons, and photons.

Our model includes a collection of N identical molecules with two electronic states (frequency ω_e and ladder operators $\hat{\sigma}_{\pm}^{(i)}$, $i \in [1, \dots, N]$), placed within the volume of a nano- or microcavity supporting a single dispersionless

EM mode (frequency $\omega_O = \omega_e = 2.5$ eV), with annihilation operator \hat{a} . The total Hamiltonian contains three different parts, as schematically depicted in Fig. 1c. First, the “bare” system \mathcal{S} accounts for the excitons within the molecules, the cavity EM mode, and their coupling, measured by the collective Rabi frequency Ω_R and treated within the rotating wave approximation (setting $\hbar = 1$),

$$\hat{H}_S = \omega_O \hat{a}^\dagger \hat{a} + \sum_{i=1}^N \omega_e \hat{\sigma}_+^{(i)} \hat{\sigma}_-^{(i)} + \frac{\Omega_R}{2\sqrt{N}} \sum_{i=1}^N (\hat{a}^\dagger \hat{\sigma}_-^{(i)} + \hat{\sigma}_+^{(i)} \hat{a}). \quad (1)$$

Direct dipole-dipole interactions at typical intermolecular distances in strong-coupling experiments only provide small corrections [31–33] and are thus neglected here for simplicity and generality. In the single-excitation subspace, \hat{H}_S is exactly solvable, with two types of eigenstates: (i) upper (UP) and lower (LP) polaritons $|\pm\rangle = (\hat{a}^\dagger |G\rangle \pm |B\rangle)/\sqrt{2}$ with frequencies $\omega_\pm = \omega_O \pm \Omega_R/2$, which result from the hybridization of the collective excitonic *bright* state $|B\rangle = (\sum_{i=1}^N \hat{\sigma}_+^{(i)} |G\rangle)/\sqrt{N}$ with the cavity EM mode (with $|G\rangle$ the global vacuum state). (ii) $N-1$ purely excitonic *dark* states (DS), $|d\rangle \in \mathcal{D}$, orthogonal to $|B\rangle$, with frequency ω_e .

The second part of the Hamiltonian describes the vibrational subspace $\mathcal{E}_v^{(i)}$ containing M_v vibrational modes for each molecule, and their elastic coupling to the excitons. The k th vibrational mode is approximated by a harmonic oscillator of frequency ω_k (valid close to the equilibrium position) with annihilation operator $\hat{b}_k^{(i)}$ and k -dependent exciton-phonon coupling strength $\lambda_k^{(i)}$,

$$\hat{H}_v = \sum_{i=1}^N \sum_{k=1}^{M_v} \omega_k \hat{b}_k^{(i)\dagger} \hat{b}_k^{(i)} + \sum_{i=1}^N \sum_{k=1}^{M_v} \lambda_k^{(i)} (\hat{b}_k^{(i)} + \hat{b}_k^{(i)\dagger}) \hat{\sigma}_+^{(i)} \hat{\sigma}_-^{(i)}. \quad (2)$$

The properties of these modes, $\{\omega_k, \lambda_k^{(i)}\}$, are encoded in the spectral density, assumed to be identical for all molecules, $J_v^{(i)}(\omega) = J_v(\omega) = \pi \sum_{k=1}^{M_v} \lambda_k^2 \delta(\omega - \omega_k)$. For Rhodamine 800 this density is extracted from the spectroscopic measurements in Ref. [34], as displayed in Fig. 1b, with vibrational frequencies located in the range $[0, 0.3]$ eV, and reorganization energy $\Delta = \int_0^\infty \frac{J_v(\omega)}{\pi\omega} d\omega \approx 35.6$ meV. While no interactions between vibrational modes are included in the model, internal vibrational decay due to interactions with the host medium is partially represented through the non-zero width of the peaks in $J_v(\omega)$. Furthermore, we have checked that the results presented below do not depend sensitively on the properties of $J_v(\omega)$.

The third part of the Hamiltonian describes radiative far-field photon modes \hat{f}_l and their coupling to the cavity EM mode, $\hat{H}_r = \sum_l \omega_l \hat{f}_l^\dagger \hat{f}_l + \eta_l (\hat{a}^\dagger \hat{f}_l + \hat{f}_l^\dagger \hat{a})$ [35]. In a way similar to vibrational modes, we introduce here the spectral density for the photonic subspace, \mathcal{E}_r , as $J_r(\omega) = \pi \sum_l \eta_l^2 \delta(\omega - \omega_l) = \kappa \omega^3 / (2\omega_O^3)$. We set the bare-cavity decay rate $\kappa = 2J_r(\omega_O)$ to 50 meV, typical for plasmonic/dielectric cavities.

For typical molecules, the large number of vibrational modes, $M_v \sim 10^2$, makes direct diagonalization of the total Hamiltonian infeasible. We resolve this by applying the TDVMPS approach. We first perform an orthogonal chain mapping of the modes in the N vibrational (green) and the free-space photon (blue) environments ($\mathcal{E}_v^{(i)}$ and \mathcal{E}_r), sketched in Fig. 1c and detailed in [36], regrouping them in chains with length $L = M_v$ with nearest-neighbor hopping, with only the first chain mode coupled to the exciton-photon subspace \mathcal{S} (red-blue) [37]. The wave function $|\psi(t)\rangle$ is represented by a tensor network [38] with maximum bond dimensions D with a structure mimicking the transformed Hamiltonian. If a single root tensor stores the system \mathcal{S} , its size scales exponentially with N , leading to a severe memory bottleneck. This scaling can be efficiently reduced while maintaining precision by decomposing $|\psi(t)\rangle$ into a *tree* tensor network, with a structure determined to minimize the entanglement between nodes [39, 40], and each final branch coupled to a single chain (see [36] for details). This allows for the treatment of $N = 16$ molecules coupled to $N + 1$ environments with $L = 350$ modes each, i.e., a system for which the full Hilbert space has a dimension of $\approx 50^{(N+1)L}$ (allowing 50 basis states per phonon mode), with $(N + 1)L = 5950$, through a wavefunction described by $\approx 10^8$ parameters. To further ameliorate memory issues for large chain mode occupations, we employ an optimal boson basis for the chain tensors, determined on the fly [41]. A more detailed description of the theoretical approach can be found in [42, 43]. We here focus on the time evolution after excitation, but note that the same approach also allows efficient calculation of the “lower polaron-polariton” [11, 25, 44, 45], as shown in [43].

We first explore single-molecule strong coupling ($N = 1$, for which there are no dark states), recently realized in plasmonic nanocavities [46, 47]. We set the initial state ($t = 0$) to the bare (vibrationally undressed) UP, $|+\rangle$, as would be produced by an on-resonance laser pulse short enough to ensure that nuclear motion can be neglected during its action. This allows to restrict the simulation to only the zero- and single-excitation subspaces of \hat{H}_S . Fig. 2 shows the time evolution of the populations $\{\rho_{GG}, \rho_{\pm\pm}\}$, extracted from the system density matrix $\hat{\rho}_S(t) = \text{Tr}_{\mathcal{E}_v, \mathcal{E}_r}\{|\psi(t)\rangle\langle\psi(t)|\}$. Details of the numerical parameters and convergence behavior can be found in the supplemental material [36]. When $\Omega_R (= 1$ eV in Fig. 2a) is much larger than the vibrational frequencies ($\omega_v^{\text{cut}} = 0.3$ eV), the bare UP (ρ_{++}) shows rapid exponential decay to the ground state (ρ_{GG}) through photon emission, with a negligible population increase of the LP. This is exactly what an approach treating \mathcal{E}_v and \mathcal{E}_r as Markovian (memory-less) baths would predict, as there are no available phonon modes that could induce transitions between UP and LP. However, already for the case $\Omega_R = 0.5$ eV, our results show a new decay pathway for the UP, which can relax through phonon

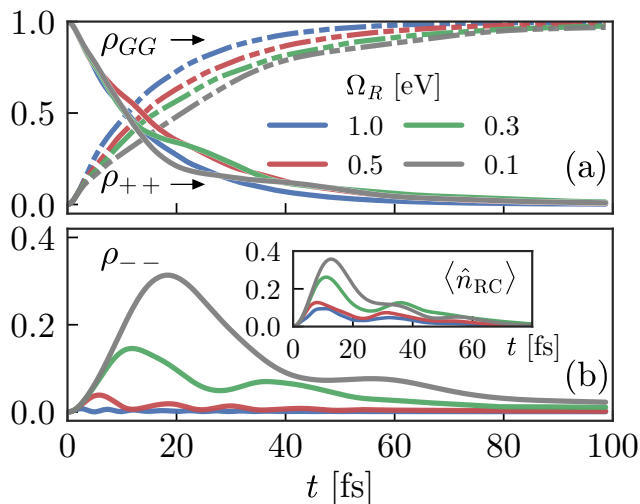


FIG. 2. Dynamics of reduced density matrix populations for a single molecule as a function of the Rabi frequency Ω_R , including (a) vacuum and upper polariton states and (b) the lower polariton. The inset in (b) shows the occupation of the collective reaction coordinate in the vibrational environment.

emission to the LP. A closer look reveals that the emission of photons, $\rho_{++} \rightarrow \rho_{GG}$, is superimposed to a coherent exchange of population between UP and LP (see Fig. 2b). Moreover, this dynamics is accompanied by a collective excitation of the vibrational modes, as displayed by the time evolution of the reaction coordinate population, $\hat{b}_{RC} = \sum_k \lambda_k \hat{b}_k / \sqrt{\sum_k \lambda_k^2}$ (inset of Fig. 2b). Neither of these effects could be reproduced by a Markovian approximation, which would lead to single-phonon transitions between polaritons at rates $\Gamma_{if}^v = 2J_v(\omega_{if})$, where $\omega_{if} = \omega_i - \omega_f$ is the transition frequency. As the Rabi splitting is larger than the largest vibrational frequency available, decay into the LP is forbidden within the Markovian limit [48]. The amplitude of these oscillations is enhanced for lower Rabi frequencies, where vibronic and photonic couplings become comparable (see cases $\Omega_R = 0.3$ eV and $\Omega_R = 0.1$ eV in Fig. 2b). Here the onset of non-exponential behavior in both ρ_{++} and ρ_{GG} is noticed, resulting in delayed photon emission. In particular, while the UP starts emitting photons immediately, the LP population is maximized after approximately one cycle of coherent oscillation of the reaction coordinate before radiative decay starts to dominate.

We next proceed to discuss the many-molecule case, in which dark states have a severe impact on the dynamics [49]. In this section we compare our results with those emerging from a standard master equation derived using the Markovian Bloch-Redfield-Wangsness (BRW) approach [50, 51], which considers solely the value of $J_v(\omega)$ at the transition frequency within the so-called secular approximation and is restricted to single-phonon transitions. We note that while it is possible to derive more advanced

Markovian and non-Markovian master equations [52–54], BRW theory already goes significantly beyond the widely employed Lindblad master equation approach, and allows clear identification of non-Markovian and multi-phonon processes in the TDVMPS simulations.

For very large Ω_R (see Fig. 3a), the UP decays mostly by photon emission. While vibrational decay to the LP is negligible, some population does reach the DS (with $\rho_{\mathcal{D}\mathcal{D}} = \sum_d \rho_{dd}$). Remarkably, while the photonic decay can be accurately determined by BRW theory, the prediction for the DS pathway disagrees with the TDVMPS calculation. BRW theory predicts $\rho_{\mathcal{D}\mathcal{D}} = \rho_{--} = 0$ as there are no phonon modes at the required transition frequencies, while TDVMPS shows that the DS reservoir is indeed populated. This demonstrates that vibration-driven decay from polaritonic states [22, 55–57] can occur efficiently even when no vibrational modes are resonant with the transition frequency, and that the decoupling from vibrational modes that is found for the LP under collective strong coupling [10, 11, 25, 43, 58] does not prevent decay of the UP.

For smaller values of the Rabi splitting, the UP-DS and DS-LP transition frequencies lie within the range of $J_v(\omega)$. Fig. 3b shows that for $\Omega_R = 0.5$ eV, coherent population transfer to the DS competes with the fast photonic decay of the UP, inducing threefold oscillations $\rho_{++} \leftrightarrow \rho_{\mathcal{D}\mathcal{D}} \leftrightarrow \rho_{--}$ that persist over more than 50 fs. For a larger number of molecules, population is “trapped” more efficiently in \mathcal{D} and subsequently decays to the LP over several hundred fs before being emitted (see [36] for a comparison with the case $N = 4$). While the intrinsic lifetimes of the LP and UP are similar due to efficient photon leakage out of the cavity, as seen in simulations initialized in the LP (not shown), the refilling from the DS leads to its population persisting over much longer timescales. This observation agrees with the long-time tails observed in strongly coupled J-aggregates [19, 59]. As the UP-DS-LP transition frequencies are not resonant with any vibration in the system (cf. Fig. 1b) the DS and LP remain unpopulated within BRW theory. In contrast, TDVMPS can represent both multi-phonon relaxation and the broadening of the polaritons due to decay, reducing the stringency of vibrational resonance conditions.

Similarly to the single-molecule case, vibrationally-driven oscillations take longer to relax for smaller Rabi frequencies. Interestingly, the numerical agreement between Markovian and non-Markovian approaches is improved in the particular case of $\Omega_R = 0.3$ eV (Fig. 3c), where the UP-DS transition is quasi-resonant with a vibrational resonance (cf. Fig. 1c). In this case, while the long-time behavior is reasonably well approximated by BRW theory, the rapid short-time oscillatory dynamics is averaged out. For even smaller Rabi frequencies, we do not observe a monotonic increase of the LP population, as opposed to the case $N = 1$. In particular, Fig. 3d displays the case $\Omega_R = 0.1$ eV, where the UP population is only

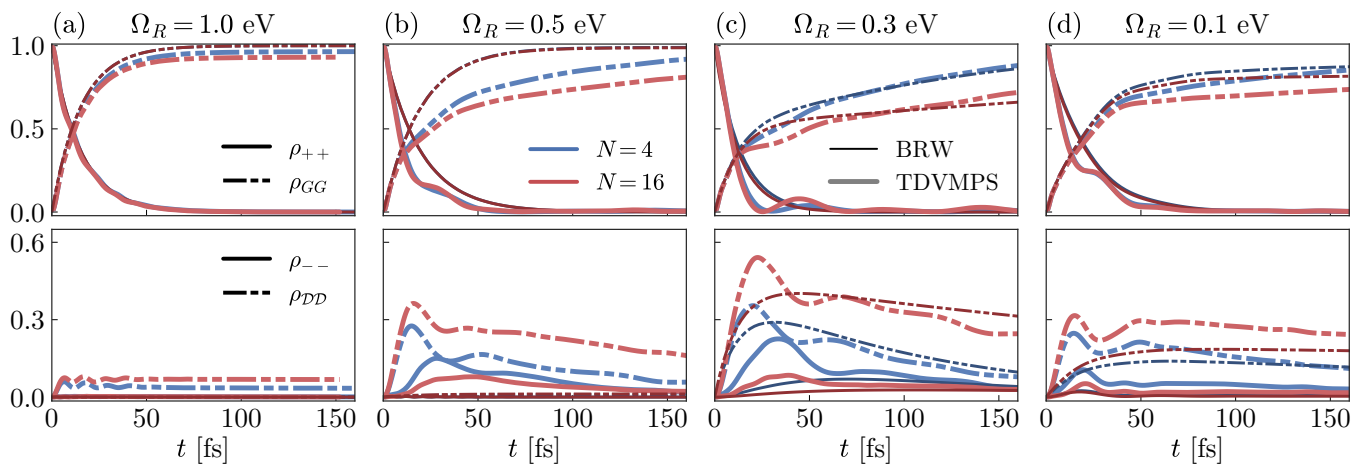


FIG. 3. Population dynamics for $N = 16$ at different Rabi frequencies (shown in titles). The occupations ρ_{GG} , ρ_{++} are displayed in the upper panels, while ρ_{--} , ρ_{DD} is shown in the lower ones, with distinctive line styles. Different colours depict the full numerical TDVMPs result and the Markovian limit calculated as described in the text.

slightly more efficiently transferred to DS and LP than for $\Omega_R = 0.5$ eV (Fig. 3b). Here the large phonon coupling leads to a rapid destruction of polariton coherence, i.e., loss of strong coupling [4].

In the supplemental material [36], we additionally compare TDVMPs with the single-mode HTC model, which has been successfully used to predict non-Markovian dynamics and energy transfer between exciton-polaritons and DS [11, 24, 44, 60, 61]. While it reproduces the dynamics in the first few fs (dominated by the reaction coordinate response) reasonably well, it consistently overestimates the coherent oscillations observed for $t \gtrsim 10$ fs. In particular, it fails to correctly predict the excitation trapping in \mathcal{D} and instead leads to enduring oscillations.

In typical organic polariton experiments, the collected far-field photons are the main source of available information. Specifically, short-time energy redistribution between polaritons could be traced by ultrafast pump-probe experiments [19, 62–64]. The final part of this work is thus devoted to the fingerprints displayed in the time-resolved emission spectrum arising from the different dynamics regimes that have been analyzed above. Thanks to the full access to the reservoir degrees of freedom provided by TDVMPs [30], emission can be retrieved from the occupation of the far-field modes $\langle \hat{n}_r(\omega_l, t) \rangle = \langle \psi(t) | \hat{f}_l^\dagger \hat{f}_l | \psi(t) \rangle$.

For very large Rabi splittings ($\Omega_R = 1$ eV), Fig. 4a shows dominant photonic emission from the UP, with a series of side lobes converging to the main emission line due to the coherent buildup of population in the free-space mode [65]. At timescales comparable to the reaction coordinate dynamics ($\tau_{RC} = 2\pi/\omega_{RC} \simeq 23$ fs), population transfer through the DS reservoir reaches the LP and its emission is observed as well, as clearly seen in cuts at the bare polariton frequencies ω_{\pm} (lower panel of Fig. 4a) that display the buildup of far-field occupation. The asymptotic growth of the photons emitted by the LP

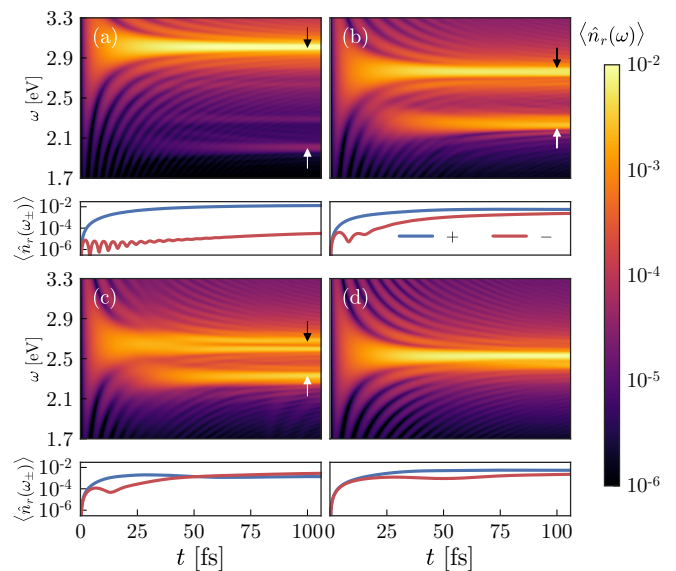


FIG. 4. Far-field photonic population as a function of frequency and time, for the same Rabi splittings as in Fig. 3 and $N = 4$. The black and white arrows in panel (a-c) point to the approximate location of the bare UP and LP. Each panel includes in the lower parts cuts at ω_{\pm} .

continues after the UP is practically depopulated, due to the continued refilling from the dark states. In addition to the vibration-free polaritons $|\pm\rangle$, emission bands at intermediate energies are visible in the spectrum. This is interpreted as due to small cavity admixtures to (vibrationally relaxed) dark states, in line with experimental observations [59, 66].

As the Rabi frequency is diminished, more efficient coupling from UP to DS increases population transfer and induces brighter emission from the LP and its vibronic sidebands. For $\Omega_R = 0.3$ eV, depicted in Fig. 4c, the

UP-DS and DS-LP transitions are close to resonant with a vibrational mode, and splitting of the emission from the UP is observed, consistent with the coherent oscillations in Fig. 3c. This is reminiscent of the splitting between vibrationally dressed and undressed polaritonic states found in the HTC model [24, 60, 61]. Finally, for $\Omega_R = 0.1$ eV (Fig. 4d), no Rabi splitting is observed, suggesting that the system is in the weak-coupling regime where no polaritons are formed.

To conclude, we have unveiled the temporal dynamics of organic polaritons. We have employed a powerful quasi-exact tree tensor network algorithm, which has enabled us to treat a highly structured reservoir of molecular vibrations and free-space emission of the cavity without additional approximations. The simulations reveal coherent vibration-driven oscillations between polaritons and dark states that are only weakly dependent on resonance conditions due to the strong exciton-phonon coupling. This demonstrates the importance of multi-phonon processes and non-Markovian dynamics in the system, which are easily underestimated or overestimated in simplified frameworks such as the Bloch-Redfield-Wangsness approximation or the Holstein-Tavis-Cummings model. In addition, the time-resolved emission spectra show fast energy relaxation to the lower polariton, on the scale of tens of femtoseconds. In contrast to Kasha's rule for bare molecules, the radiative and vibrational decays of the upper polariton are similarly fast, and its emission is clearly observed.

This work has been funded by the European Research Council (ERC-2011-AdG-290981 and ERC-2016-STG-714870), by the European Union Seventh Framework Programme under grant agreement FP7-PEOPLE-2013-CIG-618229, and the Spanish MINECO under contract MAT2014-53432-C5-5-R and the "María de Maeztu" programme for Units of Excellence in R&D (MDM-2014-0377). F.A.Y.N.S. and A.W.C. gratefully acknowledge the support of the Winton Programme for the Physics of Sustainability and EPSRC.

* johannes.feist@uam.es

† fj.garcia@uam.es

- [1] D. G. Lidzey, D. D. C. Bradley, M. S. Skolnick, T. Virgili, S. Walker, and D. M. Whittaker, "Strong Exciton-Photon Coupling in an Organic Semiconductor Microcavity," *Nature* **395**, 53 (1998).
- [2] J. Bellessa, C. Bonnard, J. C. Plenet, and J. Mugnier, "Strong Coupling between Surface Plasmons and Excitons in an Organic Semiconductor," *Phys. Rev. Lett.* **93**, 036404 (2004).
- [3] J. Dintinger, S. Klein, F. Bustos, W. L. Barnes, and T. W. Ebbesen, "Strong Coupling between Surface Plasmon-Polaritons and Organic Molecules in Subwavelength Hole Arrays," *Phys. Rev. B* **71**, 035424 (2005).
- [4] P. Törmä and W. L. Barnes, "Strong Coupling between Surface Plasmon Polaritons and Emitters: A Review," *Rep. Prog. Phys.* **78**, 013901 (2015).
- [5] Daniele Sanvitto and Stéphane Kéna-Cohen, "The Road towards Polaritonic Devices," *Nat. Mater.* **15**, 1061 (2016).
- [6] E. Orgiu, J. George, J. A. Hutchison, E. Devaux, J. F. Dayen, B. Doudin, F. Stellacci, C. Genet, J. Schachenmayer, C. Genes, G. Pupillo, P. Samorì, and T. W. Ebbesen, "Conductivity in Organic Semiconductors Hybridized with the Vacuum Field," *Nat. Mater.* **14**, 1123 (2015).
- [7] Johannes Feist and Francisco J. Garcia-Vidal, "Extraordinary Exciton Conductance Induced by Strong Coupling," *Phys. Rev. Lett.* **114**, 196402 (2015).
- [8] Johannes Schachenmayer, Claudiu Genes, Edoardo Tignone, and Guido Pupillo, "Cavity-Enhanced Transport of Excitons," *Phys. Rev. Lett.* **114**, 196403 (2015).
- [9] James A. Hutchison, Tal Schwartz, Cyriaque Genet, Eloïse Devaux, and Thomas W. Ebbesen, "Modifying Chemical Landscapes by Coupling to Vacuum Fields," *Angew. Chem.* **124**, 1624 (2012).
- [10] Javier Galego, Francisco J. Garcia-Vidal, and Johannes Feist, "Cavity-Induced Modifications of Molecular Structure in the Strong-Coupling Regime," *Phys. Rev. X* **5**, 041022 (2015).
- [11] Felipe Herrera and Frank C. Spano, "Cavity-Controlled Chemistry in Molecular Ensembles," *Phys. Rev. Lett.* **116**, 238301 (2016).
- [12] Kochise Bennett, Markus Kowalewski, and Shaul Mukamel, "Novel Photochemistry of Molecular Polaritons in Optical Cavities," *Faraday Discuss.* **194**, 259 (2016).
- [13] Johannes Flick, Christian Schäfer, Michael Ruggenthaler, Heiko Appel, and Angel Rubio, "Ab Initio Optimized Effective Potentials for Real Molecules in Optical Cavities: Photon Contributions to the Molecular Ground State," *ACS Photonics* **5**, 992 (2018).
- [14] S. R. K. Rodriguez, J. Feist, M. A. Verschuuren, F. J. García Vidal, and J. Gómez Rivas, "Thermalization and Cooling of Plasmon-Exciton Polaritons: Towards Quantum Condensation," *Phys. Rev. Lett.* **111**, 166802 (2013).
- [15] Johannes D. Plumhof, Thilo Stöferle, Lijian Mai, Ullrich Scherf, and Rainer F. Mahrt, "Room-Temperature Bose-Einstein Condensation of Cavity Exciton-Polaritons in a Polymer," *Nat. Mater.* **13**, 247 (2013).
- [16] K. S. Daskalakis, S. A. Maier, R. Murray, and S. Kéna-Cohen, "Nonlinear Interactions in an Organic Polariton Condensate," *Nat. Mater.* **13**, 271 (2014).
- [17] S. Kéna-Cohen and S. R. Forrest, "Room-Temperature Polariton Lasing in an Organic Single-Crystal Microcavity," *Nat. Photonics* **4**, 371 (2010).
- [18] Mohammad Ramezani, Alexei Halpin, Antonio I. Fernández-Domínguez, Johannes Feist, Said Rahimzadeh-Kalaleh Rodriguez, Francisco J. Garcia-Vidal, and Jaime Gómez Rivas, "Plasmon-Exciton-Polariton Lasing," *Optica* **4**, 31 (2017).
- [19] Tal Schwartz, James A. Hutchison, Jérémie Léonard, Cyriaque Genet, Stefan Haacke, and Thomas W. Ebbesen, "Polariton Dynamics under Strong Light-Molecule Coupling," *ChemPhysChem* **14**, 125 (2013).
- [20] Parinda Vasa, Wei Wang, Robert Pomraenke, Melanie Lammers, Margherita Maiuri, Cristian Manzoni, Giulio Cerullo, and Christoph Lienau, "Real-Time Observation of Ultrafast Rabi Oscillations between Excitons and Plasmons in Metal Nanostructures with J-Aggregates," *Nat. Photonics* **7**, 128 (2013).

- [21] Elad Eizner, Katherine Akulov, Tal Schwartz, and Tal Ellenbogen, “Temporal Dynamics of Localized Exciton–Polaritons in Composite Organic–Plasmonic Meta-surfaces,” *Nano Lett.* **17**, 7675 (2017).
- [22] M. Litinskaya, P. Reineker, and V. M. Agranovich, “Fast Polariton Relaxation in Strongly Coupled Organic Microcavities,” *J. Lumin.* **110**, 364 (2004).
- [23] Paolo Michetti and Giuseppe C. La Rocca, “Exciton-Phonon Scattering and Photoexcitation Dynamics in J-Aggregate Microcavities,” *Phys. Rev. B* **79**, 035325 (2009).
- [24] Felipe Herrera and Frank C. Spano, “Theory of Nanoscale Organic Cavities: The Essential Role of Vibration-Photon Dressed States,” *ACS Photonics* **5**, 65 (2018).
- [25] M. Ahsan Zeb, Peter G. Kirton, and Jonathan Keeling, “Exact States and Spectra of Vibrationally Dressed Polaritons,” *ACS Photonics* **5**, 249 (2018).
- [26] Javier Prior, Alex W. Chin, Susana F. Huelga, and Martin B. Plenio, “Efficient Simulation of Strong System-Environment Interactions,” *Phys. Rev. Lett.* **105**, 050404 (2010).
- [27] Jutho Haegeman, J. Ignacio Cirac, Tobias J. Osborne, Iztok Pižorn, Henri Verschelde, and Frank Verstraete, “Time-Dependent Variational Principle for Quantum Lattices,” *Phys. Rev. Lett.* **107**, 070601 (2011).
- [28] A. W. Chin, J. Prior, R. Rosenbach, F. Caycedo-Soler, S. F. Huelga, and M. B. Plenio, “The Role of Non-Equilibrium Vibrational Structures in Electronic Coherence and Recoherence in Pigment–Protein Complexes,” *Nat. Phys.* **9**, 113 (2013).
- [29] Michael L. Wall, Arghavan Safavi-Naini, and Ana Maria Rey, “Simulating Generic Spin-Boson Models with Matrix Product States,” *Phys. Rev. A* **94**, 053637 (2016).
- [30] Florian A. Y. N. Schröder and Alex W. Chin, “Simulating Open Quantum Dynamics with Time-Dependent Variational Matrix Product States: Towards Microscopic Correlation of Environment Dynamics and Reduced System Evolution,” *Phys. Rev. B* **93**, 075105 (2016).
- [31] Justyna A. Ćwik, Sahinur Reja, Peter B. Littlewood, and Jonathan Keeling, “Polariton Condensation with Saturable Molecules Dressed by Vibrational Modes,” *EPL Europhys. Lett.* **105**, 47009 (2014).
- [32] Carlos Gonzalez-Ballester, Johannes Feist, Eduardo Gonzalo Badía, Esteban Moreno, and Francisco J. Garcia-Vidal, “Uncoupled Dark States Can Inherit Polaritonic Properties,” *Phys. Rev. Lett.* **117**, 156402 (2016).
- [33] R. Sáez-Blázquez, J. Feist, A. I. Fernández-Domínguez, and F. J. García-Vidal, “Enhancing Photon Correlations through Plasmonic Strong Coupling,” *Optica* **4**, 1363 (2017).
- [34] N. Christensson, B. Dietzek, A. Yartsev, and T. Pullerits, “Electronic Photon Echo Spectroscopy and Vibrations,” *Vib. Spectrosc.* **53**, 2 (2010).
- [35] Note that the coherent coupling to free-space radiative modes induces a small Lamb shift in the effective cavity frequency that depends on the numerical cutoff ω_r^{cut} ($= 3.5$ eV in this work).
- [36] See Supplemental Material below, which includes Refs. [67–72], for details on the chain mapping, tree tensor networks, effects of ensemble size, a comparison with the Holstein-Tavis-Cummings model, and convergence tests.
- [37] Alex W. Chin, Susana F. Huelga, and Martin B. Plenio, “Chain Representations of Open Quantum Systems and Their Numerical Simulation with Time-Adaptive Density Matrix Renormalisation Group Methods,” in *Semiconductors and Semimetals*, Vol. 85 (Elsevier Inc., 2011) p. 115.
- [38] Ulrich Schollwöck, “The Density-Matrix Renormalization Group in the Age of Matrix Product States,” *Ann. Phys.* **326**, 96 (2011).
- [39] Szilárd Szalay, Max Pfeffer, Valentin Murg, Gergely Barcza, Frank Verstraete, Reinhold Schneider, and Örs Leggeza, “Tensor Product Methods and Entanglement Optimization for Ab Initio Quantum Chemistry,” *Int. J. Quantum Chem.* **115**, 1342 (2015).
- [40] Y.-Y. Shi, L.-M. Duan, and G Vidal, “Classical Simulation of Quantum Many-Body Systems with a Tree Tensor Network,” *Phys. Rev. A* **74**, 022320 (2006).
- [41] Cheng Guo, Andreas Weichselbaum, Jan von Delft, and Matthias Vojta, “Critical and Strong-Coupling Phases in One- and Two-Bath Spin-Boson Models,” *Phys. Rev. Lett.* **108**, 160401 (2012).
- [42] Florian A. Y. N. Schröder, David H. P. Turban, Andrew J. Musser, Nicholas D. M. Hine, and Alex W. Chin, “Multi-Dimensional Tensor Network Simulation of Open Quantum Dynamics in Singlet Fission,” [arXiv:1710.01362](https://arxiv.org/abs/1710.01362).
- [43] Javier del Pino, Florian A. Y. N. Schröder, Alex W. Chin, Johannes Feist, and Francisco J. Garcia-Vidal, “Tensor Network Simulation of Polaron-Polaritons in Organic Microcavities,” *Phys. Rev. B* **98**, 165416 (2018).
- [44] F. C. Spano, “Optical Microcavities Enhance the Exciton Coherence Length and Eliminate Vibronic Coupling in J-Aggregates,” *J. Chem. Phys.* **142**, 184707 (2015).
- [45] Ning Wu, Johannes Feist, and Francisco J. Garcia-Vidal, “When Polarons Meet Polaritons: Exciton-Vibration Interactions in Organic Molecules Strongly Coupled to Confined Light Fields,” *Phys. Rev. B* **94**, 195409 (2016).
- [46] Gülis Zengin, Göran Johansson, Peter Johansson, Tomasz J Antosiewicz, Mikael Käll, and Timur Shegai, “Approaching the Strong Coupling Limit in Single Plasmonic Nanorods Interacting with J-Aggregates,” *Sci. Rep.* **3**, 3074 (2013).
- [47] Rohit Chikkaraddy, Bart de Nijs, Felix Benz, Steven J. Barrow, Oren A. Scherman, Edina Rosta, Angela Demetriadou, Peter Fox, Ortwin Hess, and Jeremy J. Baumberg, “Single-Molecule Strong Coupling at Room Temperature in Plasmonic Nanocavities,” *Nature* **535**, 127 (2016).
- [48] Heinz-Peter Breuer and Francesco Petruccione, *The Theory of Open Quantum Systems* (Oxford University Press, 2007).
- [49] Marina Litinskaya and Peter Reineker, “Loss of Coherence of Exciton Polaritons in Inhomogeneous Organic Microcavities,” *Phys. Rev. B* **74**, 165320 (2006).
- [50] R. K. Wangsness and F. Bloch, “The Dynamical Theory of Nuclear Induction,” *Phys. Rev.* **89**, 728 (1953).
- [51] Alfred G. Redfield, “Nuclear Magnetic Resonance Saturation and Rotary Saturation in Solids,” *Phys. Rev.* **98**, 1787 (1955).
- [52] I. Wilson-Rae and A. Imamoglu, “Quantum Dot Cavity-QED in the Presence of Strong Electron-Phonon Interactions,” *Phys. Rev. B* **65**, 235311 (2002).
- [53] Dara P. S. McCutcheon and Ahsan Nazir, “Quantum Dot Rabi Rotations beyond the Weak Exciton–Phonon Coupling Regime,” *New J. Phys.* **12**, 113042 (2010).
- [54] C. Roy and S. Hughes, “Phonon-Dressed Mollow Triplet in the Regime of Cavity Quantum Electrodynamics: Excitation-Induced Dephasing and Nonperturbative Cavity Feeding Effects,” *Phys. Rev. Lett.* **106**, 247403 (2011).
- [55] David M. Coles, Niccolo Somaschi, Paolo Michetti, Caspar

- Clark, Pavlos G. Lagoudakis, Pavlos G. Savvidis, and David G. Lidzey, “Polariton-Mediated Energy Transfer between Organic Dyes in a Strongly Coupled Optical Microcavity,” *Nat. Mater.* **13**, 712 (2014).
- [56] Javier del Pino, Johannes Feist, and Francisco J. Garcia-Vidal, “Quantum Theory of Collective Strong Coupling of Molecular Vibrations with a Microcavity Mode,” *New J. Phys.* **17**, 053040 (2015).
- [57] Tomáš Neuman and Javier Aizpurua, “Origin of the Asymmetric Light Emission from Molecular Exciton-Polaritons,” [arXiv:1804.08878](https://arxiv.org/abs/1804.08878).
- [58] Javier Galego, Francisco J. Garcia-Vidal, and Johannes Feist, “Suppressing Photochemical Reactions with Quantized Light Fields,” *Nat. Commun.* **7**, 13841 (2016).
- [59] Jino George, Shaojun Wang, Thibault Chervy, Antoine Canaguier-Durand, Gael Schaeffer, Jean-Marie Lehn, James A. Hutchison, Cyriaque Genet, and Thomas W. Ebbesen, “Ultra-Strong Coupling of Molecular Materials: Spectroscopy and Dynamics,” *Faraday Discuss.* **178**, 281 (2015).
- [60] Felipe Herrera and Frank C. Spano, “Dark Vibronic Polaritons and the Spectroscopy of Organic Microcavities,” *Phys. Rev. Lett.* **118**, 223601 (2017).
- [61] Felipe Herrera and Frank C. Spano, “Absorption and Photoluminescence in Organic Cavity QED,” *Phys. Rev. A* **95**, 053867 (2017).
- [62] P. G. Savvidis, L. G. Connolly, M. S. Skolnick, D. G. Lidzey, and J. J. Baumberg, “Ultrafast Polariton Dynamics in Strongly Coupled Zinc Porphyrin Microcavities at Room Temperature,” *Phys. Rev. B* **74**, 113312 (2006).
- [63] Jung-Hoon Song, Y. He, A. V. Nurmikko, J. Tischler, and V. Bulovic, “Exciton-Polariton Dynamics in a Transparent Organic Semiconductor Microcavity,” *Phys. Rev. B* **69**, 235330 (2004).
- [64] Rudi Berera, Rienk van Grondelle, and John T. M. Kennis, “Ultrafast Transient Absorption Spectroscopy: Principles and Application to Photosynthetic Systems,” *Photosynth. Res.* **101**, 105 (2009).
- [65] Luca Argenti, Renate Pazourek, Johannes Feist, Stefan Nagele, Matthias Liertzer, Emil Persson, Joachim Burgdörfer, and Eva Lindroth, “Photoionization of Helium by Attosecond Pulses: Extraction of Spectra from Correlated Wave Functions,” *Phys. Rev. A* **87**, 053405 (2013).
- [66] Svitlana Baieva, Ossi Hakamaa, Gerrit Groenhof, Tero T. Heikkilä, and J. Jussi Toppari, “Dynamics of Strongly Coupled Modes between Surface Plasmon Polaritons and Photoactive Molecules: The Effect of the Stokes Shift,” *ACS Photonics* **4**, 28 (2017).
- [67] C. Lanczos, “An Iteration Method for the Solution of the Eigenvalue Problem of Linear Differential and Integral Operators,” *J. Res. Natl. Bur. Stand.* **45**, 255 (1950).
- [68] A. J. Leggett, S. Chakravarty, A. T. Dorsey, Matthew P. A. Fisher, Anupam Garg, and W. Zwerger, “Dynamics of the Dissipative Two-State System,” *Rev. Mod. Phys.* **59**, 1 (1987).
- [69] G. Vidal, “Entanglement Renormalization,” *Phys. Rev. Lett.* **99**, 220405 (2007).
- [70] Jutho Haegeman, Christian Lubich, Ivan Oseledets, Bart Vandereycken, and Frank Verstraete, “Unifying Time Evolution and Optimization with Matrix Product States,” *Phys. Rev. B* **94**, 165116 (2016).
- [71] Florian Alexander Yinkan Nepomuk Schröder, *Tensor Network States Simulations of Exciton-Phonon Quantum Dynamics for Applications in Artificial Light-Harvesting*, Ph.D. thesis, University of Cambridge (2017).
- [72] J. R. Johansson, P. D. Nation, and Franco Nori, “QuTiP 2: A Python Framework for the Dynamics of Open Quantum Systems,” *Comput. Phys. Commun.* **184**, 1234 (2013).

Supplemental Material

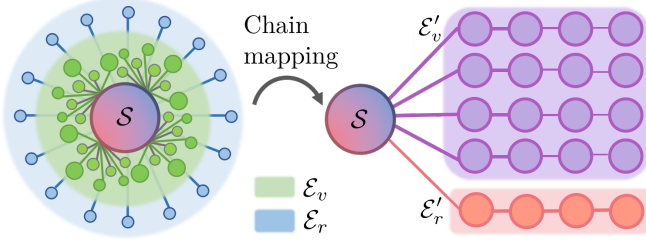


FIG. 1. Chain mapping of the multi-environment Hamiltonian in the main text to a star-structure that includes excitonic and photonic degrees of freedom in the root operator.

CHAIN MAPPING

We here give a short overview of the chain mapping that converts an environment of multiple bosonic modes with linear coupling to a system into a chain of bosonic modes with nearest-neighbor hopping, with only the first chain site coupled to the system [1]. Such an environment is described by the general Hamiltonian

$$\hat{H}_{\mathcal{E}} = \sum_{k=1}^M \left[\omega_k \hat{b}_k^\dagger \hat{b}_k + (\lambda_k \hat{O}_S^\dagger \hat{b}_k + \text{H.c.}) \right], \quad (\text{A.1})$$

where \hat{O}_S is an arbitrary system operator, and \hat{b}_k the bath oscillator annihilation operators. The environment is fully characterized through the spectral density $J(\omega) = \pi \sum_k \lambda_k^2 \delta(\omega - \omega_k)$. Rewriting $\hat{H}_{\mathcal{E}} = \hat{\beta}^\dagger \mathcal{C} \hat{\beta}$, where $\hat{\beta} = (\hat{O}_S, \hat{b}_1, \dots, \hat{b}_M)^T$, the chain mapping is obtained by tridiagonalization (e.g., with the Lanczos algorithm [2]) of the coefficient matrix $\mathcal{C} = \begin{pmatrix} 0 & \lambda \\ \lambda^\dagger & \tilde{\omega} \end{pmatrix}$, where $\lambda = (\lambda_1, \dots, \lambda_M)$ and $\tilde{\omega} = \text{diag}(\omega_1, \dots, \omega_M)$. This gives $\hat{H}_{\mathcal{E}} = \hat{\beta}^\dagger \mathcal{C} \hat{\beta}'$, with $\hat{\beta}' = (\hat{O}_S, \hat{c}_1, \dots, \hat{c}_M)^T$, and

$$C' = U^\dagger C U = \begin{pmatrix} 0 & \eta & 0 & & \\ \eta & \tilde{\omega}_1 & t_1 & & \\ 0 & t_1 & \tilde{\omega}_2 & \ddots & \\ & & \ddots & \ddots & t_{M-1} \\ & & & t_{M-1} & \tilde{\omega}_M \end{pmatrix}, \quad (\text{A.2})$$

i.e., the desired chain Hamiltonian,

$$\hat{H}_{\mathcal{E}} = \sum_{k=1}^M \tilde{\omega}_k \hat{c}_k^\dagger \hat{c}_k + \eta \left(\hat{O}_S \hat{c}_1^\dagger + \hat{O}_S^\dagger \hat{c}_1 \right) + \sum_{k=1}^{M-1} t_k \left(\hat{c}_k^\dagger \hat{c}_{k+1} + \hat{c}_{k+1}^\dagger \hat{c}_k \right), \quad (\text{A.3})$$

where the reaction coordinate that interacts with the system is given by $\hat{c}_1 = \sum_k \lambda_k \hat{b}_k / \eta$, with coupling $\eta = \sqrt{\sum_k |\lambda_k|^2}$ and frequency $\tilde{\omega}_1 = \sum_k \omega_k |\lambda_k|^2 / \eta^2$.

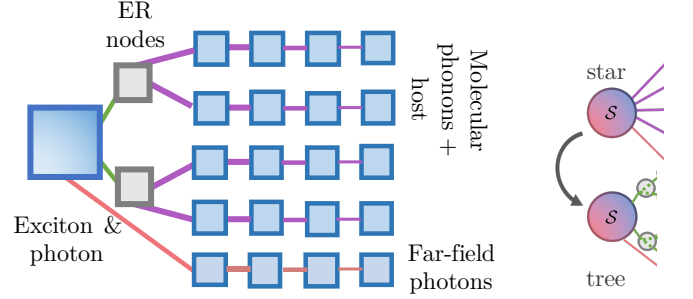


FIG. 2. Representation as a tree-like tensor network by further singular-value decompositions of the root node in the star-tensor-network that mimicks Fig. 1 (left). This requires to introduce auxiliary non-physical sites, where the acting Hamiltonian (right) presents empty operators (grey circles).

TREE TENSOR NETWORK

For the system treated in the main text (a collection of Rh800 molecules coupled to a cavity mode), the phononic bath $\mathcal{E}_v^{(i)}$ on molecule i interacts with the molecular exciton through the operator $\hat{O}_S = \sigma_+^{(i)} \sigma_-^{(i)}$, while the free-space photon modes \mathcal{E}_r interact with the cavity photon via $\hat{O}_S = a$ (in the rotating-wave approximation). For the photons, the spectral density $J_r(\omega) \propto \omega^3$ is of the Leggett form ($\propto \omega^s$, $s > 0$) [3], which enables closed expressions for all $\{\tilde{\omega}_k, t_k\}$ [1, 4].

The application of the chain mapping to all environments yields the “star” Hamiltonian sketched in Fig. 1. This Hamiltonian only contains nearest-neighbor coupling terms and thus can be efficiently implemented in tensor-network descriptions that share the same network topology [5, 6]. Since the chain mapping is linear and invertible, physical environment observables in the original basis can be obtained by applying the inverse transformation on the chain basis used in the numerical implementation. In this section, we discuss how a tree tensor network structure provides significant memory savings compared to the “naive” star network topology discussed above. In the star network, the “system” (S) is represented by a tensor with $N + 2$ dimensions (one physical index representing the coupled exciton-photon state, as well as $N + 1$ internal indices representing the coupling to the environments, with maximum bond dimension D). This leads to a severe memory bottleneck for large N as the root tensor size scales exponentially with N , $\mathcal{O}(D^{N+1})$.

In order to circumvent this exponential scaling while maintaining precision, we decompose the system into a tree tensor network state [7, 8], where each final branch is coupled only to a single chain (see Fig. 2). This in-

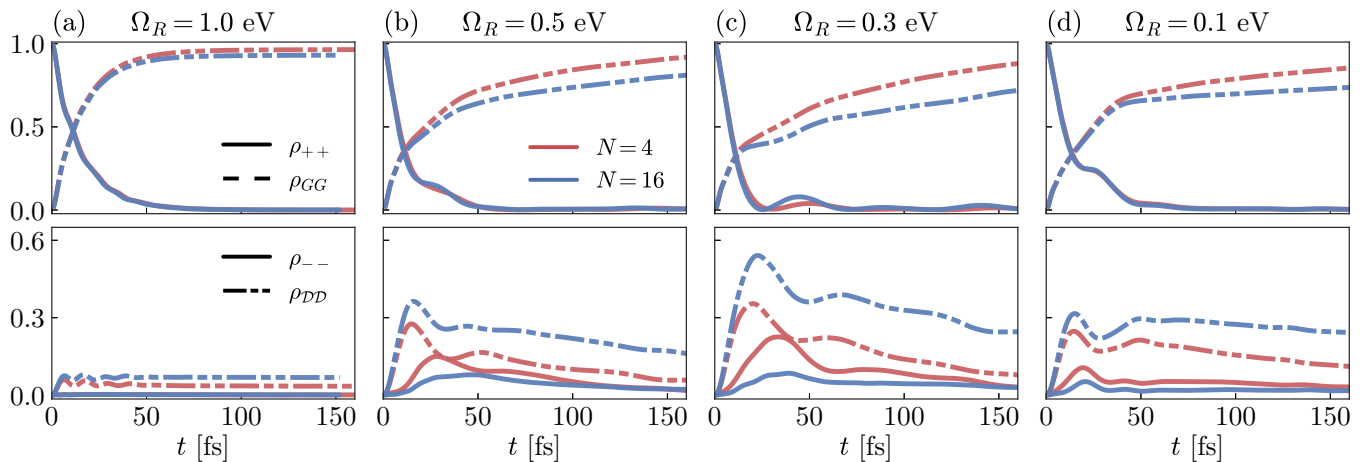


FIG. 3. Population dynamics for $N = 4$ (red) and $N = 16$ (blue) molecules for different Rabi frequencies (shown in titles). The occupations ρ_{GG} , ρ_{++} are displayed in the upper panels, while ρ_{--} , ρ_{DD} is shown in the lower ones, with distinctive line styles.

roduces additional auxiliary tensors with no physical indexes, called “entanglement renormalization tensors” [9] which take in the complete chain states and pass on a reduced number (joint states) to the system. In general, developing an efficient tree model requires an explicit analysis of the entanglement topology of the state, in essence analyzing possible regroupings and decompositions of bond legs over the star-tensor-network. The condition for this compression to be effective is that there are correlations between the chains, i.e., the sum of the reduced state entropy of each chain is greater than the joint entropy of the chains. This idea has recently been implemented to allow the simulation of multi-environment linear vibronic models constructed from ab initio parametrizations of small molecules [5]. However, in our specific case, permutation symmetry between the (identical) molecules holds. An efficient tensor network is thus given by a structure with no privileged distribution of phononic chains, i.e., the perfect binary tree in Fig. 2 with ζ levels for 2^ζ molecules. For simplicity, the environment \mathcal{E}_r is introduced as a tensor chain connected directly to the root node, as the additional leg does not increase memory storage critically.

Once the quantum wavefunction and the global Hamiltonian are represented in tree-form, the time-dependent variational principle algorithm [10] can be implemented, generalizing the single-chain algorithm [11] by recursively optimizing each of the child tensors of a given node in the tree-tensor network, and environmental chains once the leaves of the tree are reached. More details on this approach can be found in [5, 12].

ENSEMBLE SIZE EFFECTS

In this section, we discuss the effect of changing the number of molecules in the time evolution. To this effect, the system populations initialized in the vibration-free

upper polariton $|+\rangle$ for $N = 4$ and $N = 16$ molecules are shown in Fig. 3. In all cases, the increased number of dark states when increasing N leads to more efficient population transfer, both when driven through off-resonant and multi-phonon processes (for $\Omega_R = 1$ eV, Fig. 3a), and when a vibrational transition is (close to) resonant with transitions between polaritons and dark states ($\Omega_R = 0.5$ eV and $\Omega_R = 0.3$ eV, Fig. 3b-c). An analytical calculation of the rates in the Markovian limit (the Bloch-Redfield-Wangsness approach in the secular approximation) predicts that, for a Rabi frequency below the vibrational cutoff ($\Omega_R < \omega_c$), the global rate for a transition from the upper polariton into the dark-state subspace \mathcal{D} scales as $(N - 1)/N$, while the rate for the transitions $\rho_{++} \rightarrow \rho_{--}$ and $\rho_{DD} \rightarrow \rho_{--}$ is suppressed as $\sim 1/N$ [13]. However, our results in Fig. 3b,c indicate that dark-state decay happens at comparable rates for $N = 4$ and $N = 16$. Additionally, the time-dependent oscillation pattern is quite similar for $N = 4$ and $N = 16$, with the threefold oscillation $\rho_{++} \leftrightarrow \rho_{DD} \leftrightarrow \rho_{--}$ determined by the phononic reaction coordinate dynamics, but largely independent of ensemble size. For $\Omega_R = 0.1$ eV, shown in Fig. 3d, the “universality” in the early-time oscillation frequency is preserved, but in contrast to the larger Rabi splittings, the rate at which dark states decay into the lower polariton again decreases with N . We interpret this as due to the breakdown of strong coupling, which leads to the initial state $|+\rangle$ having contributions from strongly vibrationally-dressed dark states which only decay inefficiently.

COMPARISON WITH HOLSTEIN-TAVIS-CUMMINGS MODEL

In this section we first check the reliability of the numerical method by comparing the time evolution of the

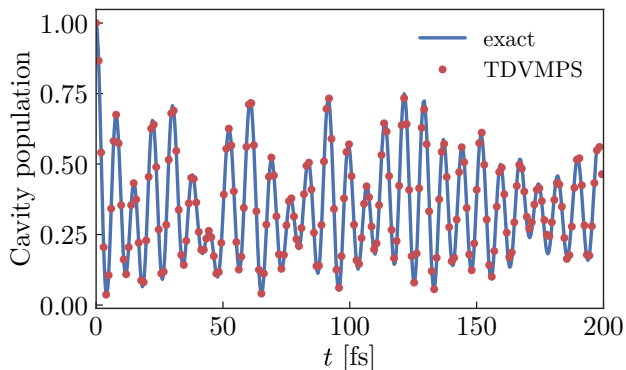


FIG. 4. Comparison of the cavity population dynamics under the single-phonon mode description of $N = 2$ molecules (HTC) between exact time propagation and a TDVMPS calculation. For this test, $\Delta = 0.112$ eV and $\tilde{\omega}_1 = 0.154$ eV.

loss-less Holstein-Tavis-Cummings (HTC) model, which only includes a single vibrational mode per molecule, via TDVMPS algorithm, with the result arising from an exact computation of the time propagation, retrieved via the open source library QuTiP [14]. The parameters of the HTC model are chosen to reproduce the reaction coordinate frequency of the Rh800 molecule ($\omega_{\text{HTC}} = \tilde{\omega}_1 = 0.181$ eV) and total reorganization energy $\lambda_{\text{HTC}} = \sqrt{\omega_{\text{HTC}}\Delta}$, with $\Delta = \sum_k \lambda_k^2/\omega_k = 0.0356$ eV. This mapping has been found to reproduce the most accurate lower phonon-polariton state [15].

As displayed by the reduced population ρ_{11} in Fig. 4, the TDVMPS time evolution almost exactly (to within the linewidth of the plot) reproduces the oscillatory features arising from the light-matter coupling and vibronic-induced effects in the exact calculation. This motivates the extension of the approach to the exact multi-mode

dynamics discussed in the main text, a regime where exact time propagation becomes unfeasible in practice. We address in the following the question of whether the full many-mode time dynamics of the system can be accounted for by means of the simplistic HTC model with parameters described above. As seen in Fig. 5a, while the HTC model reproduces the initial dynamics in the first few fs reasonably well (where the reaction coordinate could be assumed to dominate the collective response), it consistently overestimates the coherent oscillations observed for times larger than about 10 fs. In particular, it fails to correctly predict the excitation trapping in the dark state subspace and in contrast leads to enduring oscillations that are not dissipated into \mathcal{D} but only lost into photons. We have checked that choosing different parameters (e.g., $\lambda_{\text{HTC}} = \eta$) does not improve the agreement significantly (not shown).

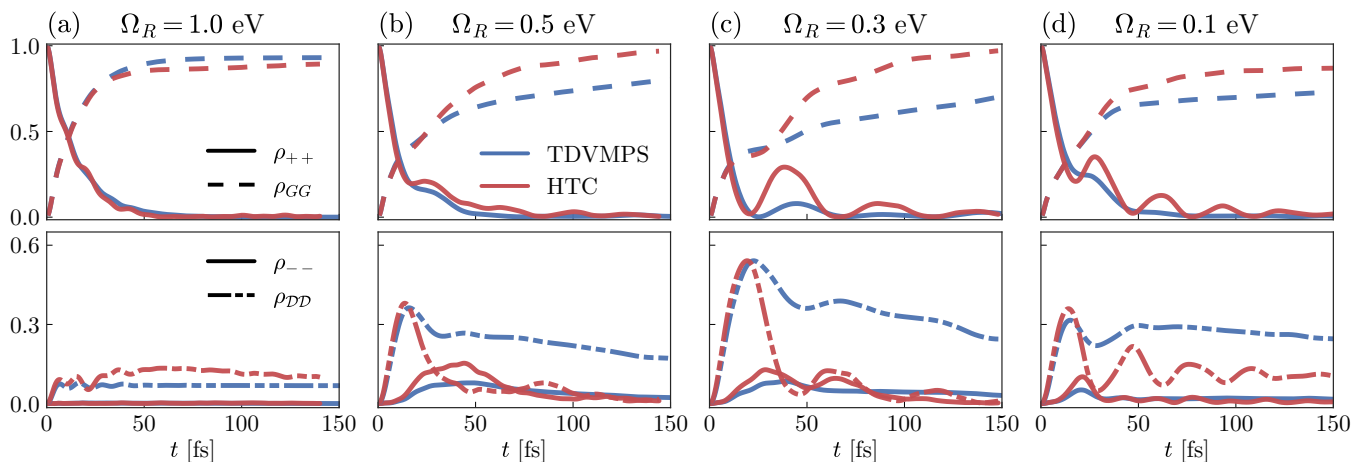


FIG. 5. Comparison of population dynamics for $N = 16$ between the full model (blue) and a single-phonon-mode description of the molecules (HTC, red). Parameters as in Fig. 3.

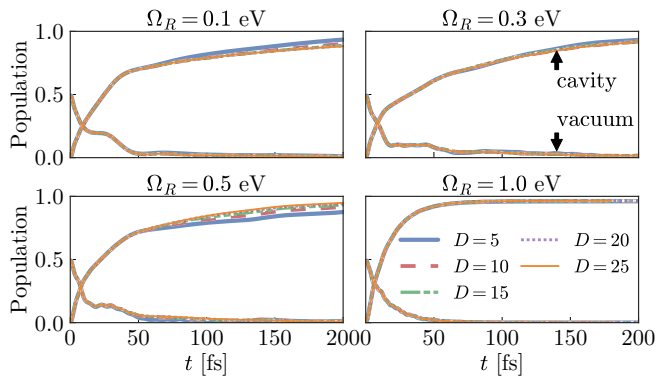


FIG. 6. Comparison of population dynamics for $N = 4$ between the full model with varying bond dimension D . Other parameters as in Fig. 3.

CONVERGENCE TESTS

Here we provide convergence checks of the tree-tensor network simulations, using the reduced population for the excited cavity (ρ_{11}) and vacuum states (ρ_{GG}) as benchmark observables. The relevant parameters in this analysis are *i*) the maximum bond dimension of the tensor network D , *ii*) the length of the chains for environments $\mathcal{E}_v, \mathcal{E}_r$, denoted L (and set equal to the number of photonic/phononic modes $L = M_v = M_r$), *iii*) the time-step Δt of time evolution, and finally *iv*) the smallest singular value kept along the calculation, denoted as sv^{tol} . For reference, the values chosen in the main text are $D = 20$, $L = 350$, $\Delta t = 0.1 \text{ eV}^{-1}$ (0.066 fs) and $\text{sv}^{\text{tol}} = 10^{-4}$. In the following analysis, we will sweep each of these parameters separately, leaving the rest at these given values. In addition, it will be convenient to define the maximum relative error between the two solutions $\rho_{GG}^{\text{sol}_1}, \rho_{GG}^{\text{sol}_2}$ where a single parameter is varied, $\epsilon = \max_t |\rho_{GG}^{\text{sol}_1}(t) - \rho_{GG}^{\text{sol}_2}(t)| / \rho_{GG}^{\text{sol}_2}(t)$.

In particular, D corresponds to the number of ‘auxiliary’ states that encode the quantum correlations between neighboring degrees of freedom, thus setting a cutoff for the maximum entanglement entropy allowed in a given bond between two physical or entanglement renormalization nodes ($S_{\text{max}} \sim \log D$ [6]). In Fig. 6, we find acceptable results for $D > 15$ for all Rabi frequencies Ω_R . Convergence of populations is remarkably more demanding in terms of D for the cases $\Omega_R = 0.5$ and 0.1 eV , where precisely Markovian (Bloch-Redfield-Wangsness) and non-Markovian time dynamics present stronger relative deviations (see main text). This observation establishes a direct link between the large amount of system-environment correlations and non-Markovianity in the time evolution. Moreover, analysis of the relative errors between the case ($D = 20$), analyzed in the main text, and the best-converged case ($D = 25$) shows a maximum deviation of $\epsilon < 1\%$ during the first 200 fs.

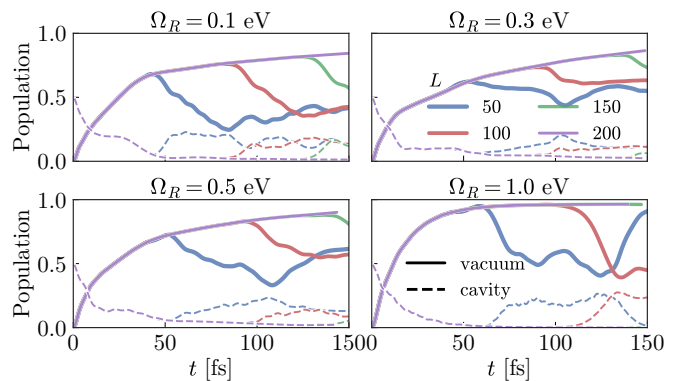


FIG. 7. Comparison of population dynamics for $N = 4$ for different chain lengths L for environments $\mathcal{E}_v, \mathcal{E}_r$. Other parameters as in Fig. 3.

Maximum dimensions D^{OBB} are also set for the bonds between chain tensors (for environments $\mathcal{E}_v^{(i)}, \mathcal{E}_r$) and the matrices mapping the optimal boson basis (OBB) into physical bosonic states [16]. In practice, a value of $D^{\text{OBB}} = 50$ is sufficient to converge the dynamics in the main text, while total phonon populations in the output of the calculation (sum over chain occupations) stay typically below 1 for all cases analyzed in the main text.

Similar results of the time dynamics as a function of the chain length L in Fig. 7 show artifacts in the density matrix $\hat{\rho}_S$ at a time that can be estimated empirically to be $\sim L$ fs, with a weak dependence on the Rabi frequency. These are caused by the arrival of the (unphysically) reflected waves at the end boundaries of photonic and phononic finite chains, which is reminiscent of TDVMPS simulations of the spin-boson model [17]. In particular, inspection of the chain populations for different environments reveals that the limiting factor is the faster velocity group (steeper dispersion curve in chain wavevector space) of photonic wavepackets. In contrast with time evolution of system observables, environmental dynamics is profoundly sensitive to the finite boundaries (e.g. reflection of a photonic excitation implies an artificial breakdown of irreversible emission dynamics after the inverse chain mapping), demanding of the order of twice this chain length to calculate populations properly. In particular, to retrieve the emission spectrum dynamics up to $t > 100$ fs in the main text, we employ a large value $L = 350$, preventing finite-size effects in the simulations.

During the simulation, the many-body state is constructed after each time-step Δt after application of the full time evolution operator. The error accrued in this propagation is discussed in detail in Ref. [11] and its references, which show that the error arises only from the numerical method employed to integrate the TDVP equations ($\mathcal{O}(\Delta t^3)$ for a left-right sweep along a single chain) [10, 17]. In addition, it has recently been pointed out that TDVMPS is accurate for local degrees of freedom

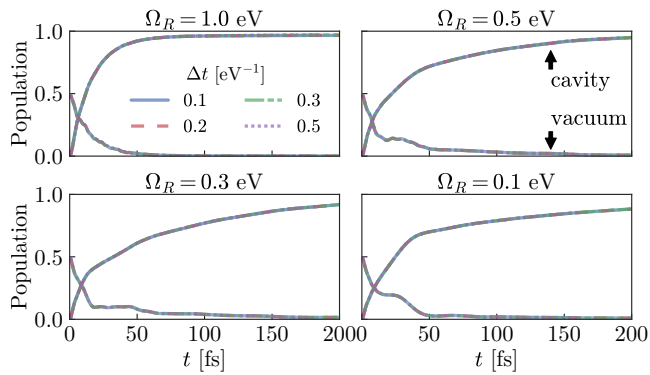


FIG. 8. Comparison of population dynamics for $N = 4$ for decreasing time step Δt . Other parameters as in Fig. 6.

at very long times even with reduced D , as the projection technique (leading to the TDVP approach) yields an effective Hamiltonian that respects underlying conservation laws in the system [18]. In order to provide a quantification of the error accrued during a global update of the tensor network by Δt , convergence plots as a function of the time-step are shown in Fig. 8. Here ρ_{GG} quickly approaches the asymptotically converged value for $\Delta t < 0.4$ eV $^{-1}$ (0.33 fs) (see Fig. 8), with relative errors that can be lowered below $\epsilon = 0.1\%$ for $\Delta t = 0.1$ eV $^{-1}$ (value in main text), for times shorter than 200 fs.

In the algorithm implementation, bond dimensions are truncated or expanded adaptively, according to the criteria that singular values $\{\nu_l\}$, which measure the entanglement between either physical or entanglement renormalization nodes (entanglement entropy $S = -\sum_l |\nu_l|^2 \log(|\nu_l|^2) \leq S_{\max}$), are truncated below a value sv^{tol} , such that only the dominant configurations required to reproduce the entangled many-body wave function are kept during the calculation. The truncation scheme above is employed similarly to the bonds between optimal boson basis matrices and the chain tensors. Fig. 9 reveals converged populations for any value below $sv^{\text{tol}} = 10^{-4}$ (value for main text calculations), and relative error analysis shows relative maximum deviations of the state populations on the order of $\epsilon \sim 1\%$ in comparison with the most compute-intensive case, where $sv^{\text{tol}} = 10^{-7}$, for times shorter than 200 fs.

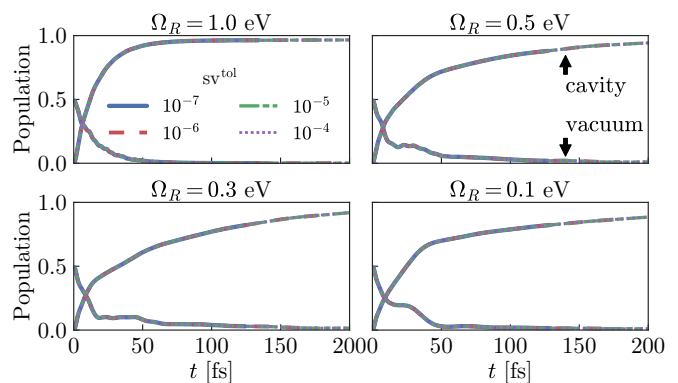


FIG. 9. Comparison of population dynamics for $N = 4$ for decreasing tolerance for singular value decomposition. Parameters as in Fig. 3.

Operators,” J. Res. Natl. Bur. Stand. **45**, 255 (1950).

* johannes.feist@uam.es

† fj.garcia@uam.es

- [1] Alex W. Chin, Susana F. Huelga, and Martin B. Plenio, “Chain Representations of Open Quantum Systems and Their Numerical Simulation with Time-Adaptive Density Matrix Renormalisation Group Methods,” in *Semicond. Semimetals*, Vol. 85 (Elsevier Inc., 2011) p. 115.
- [2] C. Lanczos, “An Iteration Method for the Solution of the Eigenvalue Problem of Linear Differential and Integral

- [3] A. J. Leggett, S. Chakravarty, A. T. Dorsey, Matthew P. A. Fisher, Anupam Garg, and W. Zwerger, “Dynamics of the Dissipative Two-State System,” *Rev. Mod. Phys.* **59**, 1 (1987).
- [4] Javier Prior, Alex W. Chin, Susana F. Huelga, and Martin B. Plenio, “Efficient Simulation of Strong System-Environment Interactions,” *Phys. Rev. Lett.* **105**, 050404 (2010).
- [5] Florian A. Y. N. Schröder, David H. P. Turban, Andrew J. Musser, Nicholas D. M. Hine, and Alex W. Chin, “Multi-Dimensional Tensor Network Simulation of Open Quantum Dynamics in Singlet Fission,” [arXiv:1710.01362](https://arxiv.org/abs/1710.01362).
- [6] Ulrich Schollwöck, “The Density-Matrix Renormalization Group in the Age of Matrix Product States,” *Ann. Phys.* **326**, 96 (2011).
- [7] Szilárd Szalay, Max Pfeffer, Valentin Murg, Gergely Barcza, Frank Verstraete, Reinhold Schneider, and Örs Leggeza, “Tensor product methods and entanglement optimization for ab initio quantum chemistry,” *Int. J. Quantum Chem.* **115**, 1342 (2015).
- [8] Y.-Y. Shi, L.-M. Duan, and G Vidal, “Classical simulation of quantum many-body systems with a tree tensor network,” *Phys. Rev. A* **74**, 022320 (2006).
- [9] G. Vidal, “Entanglement Renormalization,” *Phys. Rev. Lett.* **99**, 220405 (2007).
- [10] Jutho Haegeman, J. Ignacio Cirac, Tobias J. Osborne, Iztok Pižorn, Henri Verschelde, and Frank Verstraete, “Time-Dependent Variational Principle for Quantum Lattices,” *Phys. Rev. Lett.* **107**, 070601 (2011).
- [11] Jutho Haegeman, Christian Lubich, Ivan Oseledets, Bart Vandereycken, and Frank Verstraete, “Unifying Time Evolution and Optimization with Matrix Product States,” *Phys. Rev. B* **94**, 165116 (2016).
- [12] Florian Alexander Yinkan Nepomuk Schröder, *Tensor Network States Simulations of Exciton-Phonon Quantum Dynamics for Applications in Artificial Light-Harvesting*, Ph.D. thesis, University of Cambridge (2017).
- [13] Javier del Pino, Johannes Feist, and Francisco J. Garcia-Vidal, “Quantum Theory of Collective Strong Coupling of Molecular Vibrations with a Microcavity Mode,” *New J. Phys.* **17**, 053040 (2015).
- [14] J. R. Johansson, P. D. Nation, and Franco Nori, “QuTiP 2: A Python Framework for the Dynamics of Open Quantum

- Systems,” *Comput. Phys. Commun.* **184**, 1234 (2013).
- [15] Javier del Pino, Florian A. Y. N. Schröder, Alex W. Chin, Johannes Feist, and Francisco J. Garcia-Vidal, “Tensor network simulation of polaron-polaritons in organic microcavities,” *Phys. Rev. B* **98**, 165416 (2018).
- [16] Cheng Guo, Andreas Weichselbaum, Jan von Delft, and Matthias Vojta, “Critical and Strong-Coupling Phases in One- and Two-Bath Spin-Boson Models,” *Phys. Rev. Lett.* **108**, 160401 (2012).
- [17] Florian A. Y. N. Schröder and Alex W. Chin, “Simulating Open Quantum Dynamics with Time-Dependent Variational Matrix Product States: Towards Microscopic Correlation of Environment Dynamics and Reduced System Evolution,” *Phys. Rev. B* **93**, 075105 (2016).
- [18] Eyal Leviatan, Frank Pollmann, Jens H. Bardarson, David A. Huse, and Ehud Altman, “Quantum Thermalization Dynamics with Matrix-Product States,” [arXiv:1702.08894](https://arxiv.org/abs/1702.08894).